On the Applicability of Numerical Quadrature for Double Surface Integrals at 5G Frequencies

Mario Cvetković, *Member, IEEE,* Dragan Poljak, *Senior Member, IEEE,* Ante Lojić Kapetanović, *Student Member, IEEE,* and Hrvoje Dodig, *Member, IEEE*

***Abstract*—The human exposure assessment to wireless communications systems including the fifth generation (5G) mobile systems is related to determining the specific absorption rate (SAR) or the absorbed power density (APD). The assessment of both quantities requires the use of various numerical techniques, including moments method (MoM). As the use of MoM results in a fully populated system matrix, a tremendous computational cost is incurred, both in terms of matrix fill time and memory allocation, as the matrix size is directly related to frequency of the problem. This paper investigates the applicability of numerical integration at frequencies related to 5G. The novelty of this work is related to the comprehensive set of tests of various combination of source and observation triangles using the developed unit cube test. A number of convergence tests were performed to investigate the effects of the increasing frequency and the discretization scheme on the numerical solution, as well as to determine how to curb the computational requirements by the proficient use of numerical integration. The results show that in the lower GHz range, lower integration orders could be used, resulting in the decrease of matrix fill time without loss of solution accuracy.**

***Index Terms*—Dunavant rules; integral equation formulation; numerical integration; 5G frequencies; computational cost.**

I. INTRODUCTION

THE mobile communication systems fifth generation (5G) represents the significant evolution over the previous 4G LTE networks both in terms of high transmission data rates and overall network capacity as well as a very low latency. It is expected that 5G networks will facilitate nearly instantaneous connectivity to multibillion devices based on the use of millimeter waves operating in the GHz frequency range, but also on the use of beam steering technologies such as massive multiple input, multiple output (MIMO) antenna systems.

However, the extensive use of new MIMO antenna systems comprising a high number of antenna elements will most definitely result in the public concern due to possible negative health effects. Compared to electromagnetic (EM) radiation in the radio frequency (RF) range, the thermal effects related to the mm-waves from the GHz part of the spectrum are limited to the body surface due to small skin effect and low penetration depth. Nevertheless, rather recently, IEEE standard [1] in 2019 and ICNIRP guidelines [2] in 2020, respectively, have been revised, in order to assure the compliance with the basic restrictions and consequently to ensure the safety of humans due to exposure to EM fields. Regardless of basic restriction quantity, defined by the specific absorption rate (SAR) in the range of up to 6 GHz, or the absorbed power density (APD) for frequencies above 6 GHz, the assessment of both quantities requires the use of advanced computational methods.

Recently, integral equation based methods coupled with stochastic approach resurfaced as one of the means for solving high frequency electromagnetic-thermal dosimetry problems [3], [4]. Unfortunately, if formulations based on the use of integral equation are utilized, the accuracy of the numerical solution will be impacted by the precision with which the matrix system elements are calculated. The numerical integration is used most often to solve various double surface integrals, whereas the calculation speed and solution accuracy should be taken into account. It should be emphasized that in most cases some compromise solution between the numerical efficiency and accuracy is required.

It is a well known fact that one of the disadvantages of using integral equation formulations is they result in a fully populated system matrix. The matrix filling and the solving of system matrix represent the two time-consuming operations required by moments method (MoM) code with N unknowns [5]. In case of wire structures, these operations are of $O(N^2)$ for the former, and $O(N^3)$ for the latter, when direct solvers are used. However, in practice, matrix filling often requires more time spent. Since number of unknowns N is proportional to kd, with k and d being wave number and wire length, respectively, the asymptotic cost of these operations is of $O([kd]^3)$, clearly indicating the frequency scaling feature of the algorithm. Compared to wires, the asymptotic computational cost for surfaces is even more expensive, i.e. of $O([kd]^6)$, with matrix filling again dominating the computational runtime for most problems. On the other hand, the memory requirements for surfaces are of $O([kd]^4)$.

Additional thing to keep in mind is the system matrix size, as large matrices are impossible to directly solve, e.g. via Gaussian elimination. In these cases, the iterative procedure is required such as a generalized minimum residual method (GMRES) [6].

In recent years the graphics processing unit (GPU) has

Manuscript received November 30, 2021; revised January 13, 2022. Date of publication February 25, 2022. Date of current version February 25, 2022.

The part of this paper was presented at the International Conference on Software, Telecommunications and Computer Networks (SoftCOM) 2021.

M. Cvetković, D. Poljak, and A. Lojić Kapetanović are with the Faculty of Electrical Engineering, Mechanical Engineering and Naval Architecture, University of Split, 21000 Split, Croatia. H. Dodig is with the Faculty of Maritime Studies, University of Split, 21000 Split, Croatia. Corresponding author: M. Cvetković (mcvetkov@fesb.hr).

Digital Object Identifier (DOI): 10.24138/jcomss-2021-0183

become more often used as another important computational resource, due to GPU's computational potential compared to conventional central processing unit (CPU). Various examples of problems tackled by the finite difference time domain (FDTD) method utilizing the GPUs, can be found in [7]. More important, the graphics cards have been previously utilized in accelerating the conventional MoM calculations both in terms of filling time and splitting algorithm [8]. However, additional effort is required when using GPU, as specialized adaptation of the code is necessary, such as rewriting one's code in CUDA or other languages.

Therefore, instead of immediate paradigm shift from CPU-based to GPU-based computations, the investigation carried out in this paper is on the efficient utilization of a conventional MoM code by applying proficient numerical integration rules without sacrificing the accuracy of the approach.

It should be noted there are many interesting papers dealing with the precision of the particular integrals' numerical solution, e.g. [9]–[11], while the work presented here is related to application of pure numerical quadrature, presented, in authors opinion, in a unique way using the developed unit cube test, as well as the (P, Q)-square convergence visualization that can be considered a novelty.

This paper should be considered as an extension of two conference papers published in [12] and [13]. In first publication [12], the unit cube test was presented for testing various combinations of double surface integrals arising in the frequency domain integral formulations, while second publication [13] is on the investigation of numerical integration using said cube test. The results reported both in [12] and [13] are further extended with additional computational examples given here. In the present paper, the investigation of applicability of numerical quadrature to the solution of double surface integral related to the magnetic vector potential is tested on the combination of far and near terms, both in cases of coplanar and orthogonal triangle pairs. The numerical solution convergence of double surface integral is tested at several 5G frequencies currently utilized or to be used in Croatia (0.7 GHz, 3.6 GHz, 26 GHz, 90 GHz), as well as 6 GHz, considered as the transition frequency in the safety standards [3]. Moreover, extensive tests have been carried out to determine the effects of increasing frequency and surface discretization, respectively, both in terms of quadrature precision as well as computational requirements. The numerical study carried out in this work could found its application in the assessment procedures related to human safety to electromagnetic fields, by providing some guidelines related to the application of numerical quadrature as well as its potential applicability when very high frequencies are considered (such as in 5G).

The paper is organized as follows: following the introductory part, the mathematical background is given in second section including a brief descriptions of the used integral formulation, a numerical approach to double surface integral as well as a unit cube test and Dunavant's quadrature rules, respectively. The following section presents the results of the extensive convergence tests with the accompanying discussion. In the fourth and also the final part the concluding remarks are given.

II. MATHEMATICAL BACKGROUND

In frequency domain surface integral equation (SIE) formulations, the complex surface geometry of a problem is most commonly described using the triangular elements or patches. This enables the use of a so called Rao-Wilton-Glisson (RWG) basis functions particularly developed for triangles [14].

A. Surface Integral Equation Formulation

This work is based on the frequency domain formulation for the homogeneous penetrable scatterer. The electric field integral equation (EFIE) can be derived from the use of equivalence theorem at the scatterer's surface and the application of appropriate boundary conditions (BC):

$$\left[-\vec{E}_n^{sca}(\vec{J},\vec{M})\right]_{tan} = \begin{cases} \left[\vec{E}^{inc}\right]_{tan}, & i=1 \\ 0, & i=2 \end{cases} \tag{1}$$

where E^{inc} represents the known incident electric field while E^{sca} is the field scattered from the surface.

The tangential component of the scattered electric field can be written in terms of the equivalent surface electric and magnetic currents, $\vec{J}$ and $\vec{M}$, respectively, which, in turn, can be expanded using a linear combination of basis functions. As the surface of scatterer is represented by triangular patches, $\vec{J}$ is expanded by the RWG basis functions [14], while $\vec{M}$ is expanded by the orthogonal functions $\hat{n}\times$RWG, as follows:

$$\vec{J}(\vec{r}) = \sum_{n=1}^{N} J_n \vec{f}_n(\vec{r}); \quad \vec{M}(\vec{r}) = \sum_{n=1}^{N} M_n \vec{g}_n(\vec{r}) \tag{2}$$

where J_n and M_n are coefficients to be determined, while N denotes the number of elements used to discretize the surface S of a scatterer.

SIE formulation of the problem via EFIE can be numerically solved, e.g. using an efficient MoM scheme reported in [15]. Examples of application of a SIE based formulation include models of pediatric patients in e.g. transcranial magnetic stimulation (TMS) [16] or electromagnetic-thermal dosimetry [17], or even in a stochastic dosimetry of the human brain [18]. More details on the particular application can be found in corresponding papers [16]–[18].

Multiplying (1) by test functions $\vec{f}_m$, where $\vec{f}_m = \vec{f}_n$, and integrating over the scatterer surface S, followed by some additional steps [15], [19], results in the following integral equations set:

$$\sum_{n=1}^{N}\left(j\omega\mu_i A_{mn,i} + \frac{j}{\omega\varepsilon_i} B_{mn,i}\right) J_n + \\ + \sum_{n=1}^{N}\left(C_{mn,i} + D_{mn,i}\right) M_n = \begin{cases} V_m & ,i=1 \\ 0 & ,i=2 \end{cases} \tag{3}$$

where A_{mn}, B_{mn}, C_{mn}, and D_{mn} denote various surface integrals, while $i = 1, 2$ indicate the regions exterior and interior to the scatterer, respectively. The indices m and n denote the source and observation triangles, respectively.

Object's material properties are taken into account via μ and ε, representing permeability and permittivity, respectively.

The set of integral equations (3) can be written more compactly in the matrix form as

$$[\mathbf{Z}] \cdot \{\mathbf{I}\} = \{\mathbf{V}\} \tag{4}$$

where the size of system matrix $\mathbf{Z}$ is $2N \times 2N$, while the size of source vector $\mathbf{V}$ is $2N$, as illustrated on Fig. 1. It should be emphasized that the system matrix $\mathbf{Z}$ formed in this manner represents a fully populated matrix [4], as this is a well known drawback of integral equation formulations.

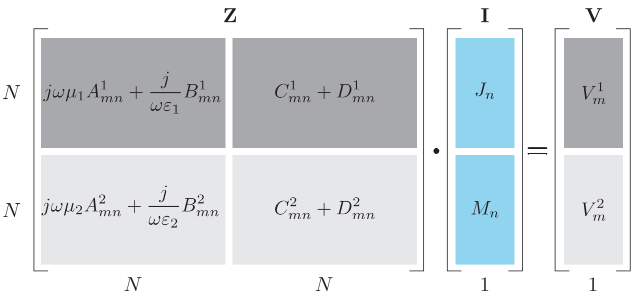

Fig. 1. The size of MoM system matrix [4]. Column vector $\mathbf{I}$ contains unknown coefficients used to determine equivalent surface electric and magnetic currents $\vec{J}$ and $\vec{M}$.

B. Numerical Integration of Double Surface Integrals

In order to determine the elements of the system matrix, it is necessary to solve various surface integrals appearing in (3). One of the double surface integrals, whose numerical solution is considered in this work, is of the following form:

$$A_{mn} = \iint_S \vec{f}_m(\vec{r}) \cdot \iint_{S'} \vec{f}_n(\vec{r}\,')G(\vec{r},\vec{r}\,')\,dS'\,dS \tag{5}$$

where $\vec{f}_m$ is test function, and $\vec{f}_n = \vec{f}_m$ represents basis function expanded over triangles. Observation and source points are denoted by $\vec{r}$ and $\vec{r}\,'$, respectively. RWG function is used as basis function [14]:

$$\vec{f}^{\pm}_n(\vec{r}) = \begin{cases} \dfrac{l_n}{2A^{\pm}_n}\vec{\rho}^{\,\pm}_n & , \vec{r} \in T^{\pm}_n \\ 0 & , \vec{r} \notin T^{\pm}_n \end{cases} \tag{6}$$

where l_n is the shared edge length at the interface between triangles T^+_n and T^-_n, while A^+_n and A^-_n denote the surface areas of triangles. Vector $\vec{\rho}^{\,+}_n = \vec{r} - \vec{r}^{\,+}_n$ is directed from free vertex of T^+_n while $\vec{\rho}^{\,-}_n = \vec{r}^{\,-}_n - \vec{r}$ is directed towards free vertex of T^-_n.

Integral (5) includes Green's function for the homogeneous medium given by:

$$G(\vec{r},\vec{r}\,') = \frac{e^{-jkR}}{4\pi R}; \qquad R = |\vec{r} - \vec{r}\,'| \tag{7}$$

where R is the distance from observation to source point, while k denotes the wave number.

Depending on the distance between source and observation triangles, T_m and T_n respectively, specific solution approach to the integral (5) is necessary.

In case when observation and source triangles are far enough, simple numerical integration suffices. On the other hand, in case of near terms, that is, when the triangles are close to each other and/or are sharing a vertex or an edge, usually the combination of analytical and numerical integration is used. Some authors suggest purely numerical integration [20], [21] also in the case of near triangles. In that situation, it is then customary to choose one sampling point from the outer triangle corresponding to numerical quadrature order of $M = 1$, where the observation point is placed at the center of a triangle. Unfortunately, due to kernel singularity, this approach will result in numerical instability, as shown in our previous work for integrals of the form D_{mn}, [22].

The investigation carried out in this work is related to evaluation of integral (5) using the numerical procedure (Gaussian quadrature). In total, four combinations of source and observation triangles are considered in this work, as depicted on Fig. 2.

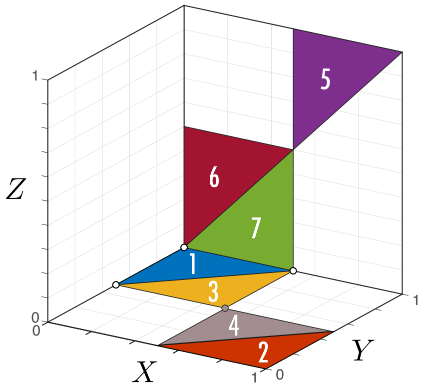

Fig. 2. Unit cube for testing various triangle combinations. Coplanar and orthogonal, far and near triangle combinations, respectively, are considered: $(1-2)$, $(1-3)$, $(1-5)$, $(1-7)$.

Triangles numbered 1 and 2 $(1-2)$ are considered as coplanar far combination (far terms), while triangles 1 and 3 $(1-3)$ denote the coplanar near combination (near terms). Furthermore, triangle combinations numbered 1 and 5 $(1-5)$ and 1 and 7 $(1-7)$ represent the orthogonal far and near terms, respectively.

Inserting (6) and (7) into (5), the double surface integral (5) can be written as

$$A_{mn} = \iint_S \frac{l_m}{2A^{\pm}_m}\vec{\rho}^{\,\pm}_m(\vec{r}) \cdot \iint_{S'} \frac{l_n}{2A^{\pm}_n}\vec{\rho}^{\,\pm}_n(\vec{r}\,')\frac{e^{-jkR}}{4\pi R}\,dS'\,dS \tag{8}$$

Both surface integrals from (8) can be approximated by a weighted coefficients sum, written on a triangular domain as:

$$\iint_T f(\alpha,\beta,\gamma)\,dS \approx A\sum_{i=1}^{N} w_i(\alpha_i,\beta_i,\gamma_i)f(\alpha_i,\beta_i,\gamma_i) \tag{9}$$

where A denote the triangle area, $w_i(\alpha_i, \beta_i, \gamma_i)$ are weighting coefficients normalized to triangle area, while α_i, β_i, and γ_i are local or simplex coordinates (defined on the unit triangle).

Utilizing (9) in (8), the following is obtained:

$$A_{mn} = \frac{l_m l_n}{16\pi A_m^{\pm} A_n^{\pm}} A_m^{\pm} \sum_{p=1}^{M} w_p \vec{\rho}_m^{\,\pm}(\vec{r}_p) \cdot$$

$$\cdot\, A_n^{\pm} \sum_{q=1}^{N} w_q \vec{\rho}_n^{\,\pm}(\vec{r}_q^{\,\prime}) \frac{e^{-jkR_{pq}}}{R_{pq}} \qquad (10)$$

while, after some cancellation and rearranging, the resulting expression is obtained:

$$A_{mn} = \frac{l_m l_n}{16\pi} \sum_{p=1}^{M} \sum_{q=1}^{N} w_p w_q \vec{\rho}_m^{\,\pm}(\vec{r}_p) \cdot \vec{\rho}_n^{\,\pm}(\vec{r}_q^{\,\prime}) \frac{e^{-jkR_{pq}}}{R_{pq}} \qquad (11)$$

with $R_{pq} = |\vec{r}_p - \vec{r}_q^{\,\prime}|$, where $\vec{r}_p$, $\vec{r}_q^{\,\prime}$, w_p and w_q denote the location of Gaussian points and weights for the source and observation triangles, respectively. M and N, represent the number of integration points for the source and observation triangle, respectively, dependent on the order of integration, $P = 1, \ldots, 20$, and $Q = 1, \ldots, 20$.

C. *Dunavant's Quadrature Rules for Triangles*

Dunavant's symmetric quadrature rules for triangles are utilized in this work. The quadrature rules of degree up to $P = 20$, with associated quadrature points and weighting coefficients can be found in [23], while the examples of symmetric location of quadrature points on the unit triangle are depicted on Fig. 3.

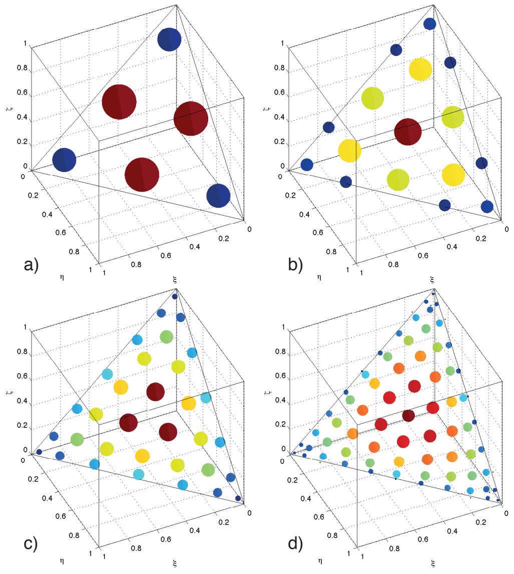

Fig. 3. The location of quadrature points on the unit triangle and the associated weights for several selected Dunavant's rules. P = integration order, n = number of points: a) $P = 4$, $n = 6$, b) $P = 8$, $n = 16$, c) $P = 12$, $n = 33$, d) $P = 20$, $n = 79$.

While there are many other rules available [24]–[28], Dunavant's rules are nowadays most frequently used integration rules for triangles, and similar to classical Gaussian quadratures, an n-point rule is exact for all polynomials of orders up to $2n - 1$, [27]. Although some of the rules have undesirable features such as nodes position outside the triangle and negative weights, Dunavant's rules are optimal in the sense that for a given rule, the number of nodes used is close to or even theoretically equal to the smallest possible value [29], which makes them highly efficient for problems requiring solutions to a large number of integrals. Furthermore, these rules use the symmetrical position of the integration nodes with respect to the vertices of the triangles, thus eliminating possible variations in the order in which they are assigned [29].

Using all the possible combinations of integration orders $P = 1, \ldots, 20$ and $Q = 1, \ldots, 20$, for the source and the observation triangles, the double surface integral (5) is solved using (11).

D. *Unit Cube Test*

The unit cube test, depicted on Fig. 2, utilized for testing the interaction between source and observation triangles, was introduced in [12]. The unit cube is meshed using 48 triangular patches, with 8 isosceles triangles on each cube side. Utilizing the cubical shape, various combinations of coplanar and orthogonal triangles could be tested, as previously mentioned. Furthermore, the unit cube and the associated mesh can be easily scaled to facilitate testing of numerical integration at various frequencies of interest.

Figure 4 illustrates the comparison of triangular element size when unit cube scale is halved in several iteration steps ($n = 1, \ldots, 8$). The discretization steps numbered $n = 4, 5, 6, 7, 8$ are latter denoted as: $1/8$, $1/16$, $1/32$, $1/64$, and $1/128$, discretization schemes, respectively.

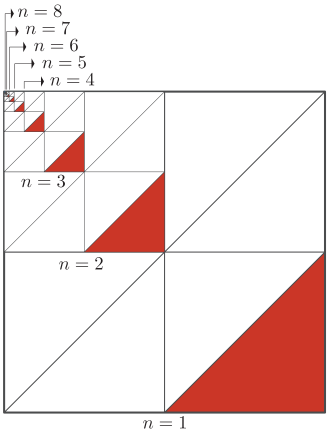

Fig. 4. Illustration of triangular element size on one side of unit qube, depending on the scaling iteration number $n = 1, \ldots, 8$.

The number of triangles per unit cube side, the total number of RWG elements, as well as other parameters of unit cube, are given in Table I.

III. RESULTS AND DISCUSSION

Utilizing the unit cube test, the following results are obtained. The first set of results are obtained without scalling of the unit cube geometry to ascertain the effects of the increased frequency. Those are followed by the results obtained using various geometry scalling in order to determine the appropriate discretization scheme suitable for the particular frequency. The final set of results are given in terms of relative error calculated for different utilized frequencies, discretization schemes and triangle combinations.

A. Visualizing Convergence using (P, Q)-square

Before going into more details, it would be beneficial to first explain how the obtained results are to be interpreted. To this end, we would like to draw the readers attention to Fig. 5.

The results depicted in Fig. 5 denote the numerical solution of double surface integral (5) in cases of far triangles and near triangles sharing an edge, numbered $(1-2)$ and $(1-3)$, respectively [12]. The results are obtained using varying integration orders P and Q for source and observation triangles, respectively, with $P = 1, \ldots, 20$ and $Q = 1, \ldots, 20$.

The unit cube is scaled such that $ka = const.$, where $a = \lambda/5$ and $b = a/2$. The cube length is denoted by a, the length of triangle edge by b, while λ is the wavelength. Thus, for a constant electrical length of cube, irrespective of frequency (tested in the frequency range from 300 MHz to 90 GHz), the solution practically converges identically.

The results for the far triangle combination, depicted on Fig. 5a), show that the increasing number of integration points results in the convergence both on the real and imaginary part of the solution. These same results are also visualized on Fig. 5b) where the convergence is represented by the grey colour shade on a (P, Q)-square, where the increase of integration order is from left to right for Q, and from top to bottom for P. It should be mentioned that the gray colour itself is not essential when considering the (P, Q)-square, but, rather, the colour of the complete (P, Q)-square is. If the shade of gray becomes uniform - when moving from top left to bottom right - the solution converges, as evidenced also on Fig. 5a).

On the other hand, the checkered pattern of (P, Q)-square indicates that the convergence is not guaranteed. This is illustrated on Fig. 5c) in case of near triangles combination. When purely numerical approach is used, as seen on Fig. 5c), at low integration orders, rather erratic behavior is evident on the real part of the solution. Compared to that, when the integration orders on both triangles are increased, the solution starts to converge. This very slow convergence of the solution can be seen by the checkered pattern, as shown on Fig. 5d).

B. The Effect of Increasing Frequency

The first set of results, shown on Fig. 6, are obtained at the following frequencies: 0.7 GHz, 3.6 GHz, 6 GHz, 26 GHz, 90 GHz. All results are obtained without the previous scaling of unit cube geometry.

As seen from Fig. 6, the convergence of real and imaginary parts of integral A_{mn} are depicted using (P,Q)-square, with respect to utilized frequency. Four triangle pair combinations are considered, namely: coplanar far terms $(1-2)$, coplanar near terms $(1-3)$, orthogonal far terms $(1-5)$, and orthogonal near terms $(1-7)$.

At lowest considered 5G frequency of 0.7 GHz, it is evident that, in the case of far terms, both coplanar and orthogonal, much lower integration orders could be used $(P = 3, 4, 5; Q = 3, 4, 5)$. In case of the near terms, on the other hand, although the imaginary part of the solution converges at lower integration order, the real part does not, hence, higher number of integration points should be used.

As the frequency increases, at 3.6 GHz and 6 GHz, checkered pattern becomes evident at lower values of P and Q, even in case of the far triangle interactions, indicating that higher integration orders should be utilized. Compared to that, the near triangle interactions does not show convergence until the highest integration orders are utilized $(P = 15-20; Q = 15-20)$.

Finally, in case of the highest frequencies, i.e. 26 GHz and 90 GHz, it is obvious that even the highest available integration order in case of far terms interaction is not sufficient to obtain the convergence. These results were expected, as it is well known that the dimensions of the utilized mesh should be at least comparable to the wavelength at particular frequency. In case of 26 GHz, the corresponding wavelength is 1.15 cm, i.e. significantly lower than the utilized triangle size (50 cm). For the comparison, at 0.7 GHz, the wavelength of EM wave (42.8 cm) is comparable to the triangle size.

Thus, to obtain a more reliable results, it is necessary first to discretize the mesh appropriately.

C. The Effect of Surface Discretization

The following set of results, shown on Figs. 7–9, are related to the effects of the surface discretization. The double surface integral (5) is again solved implementing the numerical quadrature rules using varying integration orders, utilizing several discretization schemes of the unit cube: $1/8$, $1/16$, $1/32$, $1/64$, and $1/128$. Each row from Figs. 7–9 illustrates the convergence for one of the particular combination of triangles, as previously explained. The results are obtained at the following frequencies: 3.6 GHz, 26 GHz and 90 GHz.

As seen from Figs. 7–9, as the frequency increases, much finer discretization should be used in order to ensure the convergence of the results. In case of the near terms, the checkered pattern is again obvious, however, it emerges only on the real part of the solution, while the imaginary part of the solution converges even at the lowest orders of integration.

If the discretization is adequate ($1/32$, $1/64$), as e.g. the results from Figs. 9c) and 9d) suggest, lower integration orders could be used for far terms, but also the integration of near terms could be to a certain extent utilized even at the highest considered frequency (90 GHz). Furthermore, basically the behavior (i.e. convergence) of solution's real part should determine the convenient integration order, as the convergence of the imaginary part is much smoother.

To summarize, if coarser mesh is utilized ($1/8$ and $1/16$), the convergence of the solution at higher frequencies (26 GHz

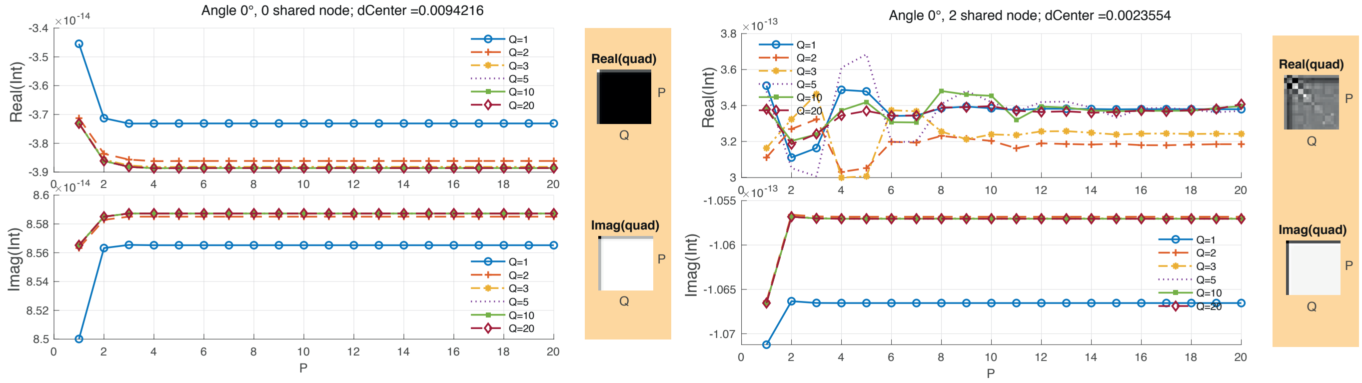

a) b) c) d)

Fig. 5. Convergence of real and imaginary part of integral using several quadrature orders ($Q = 1, 2, 3, 5, 10, 20$), a) Far terms, c) Near terms. Visualization of b) Far and d) Near triangles interaction using a so called (P, Q)-square. Adapted from [12].

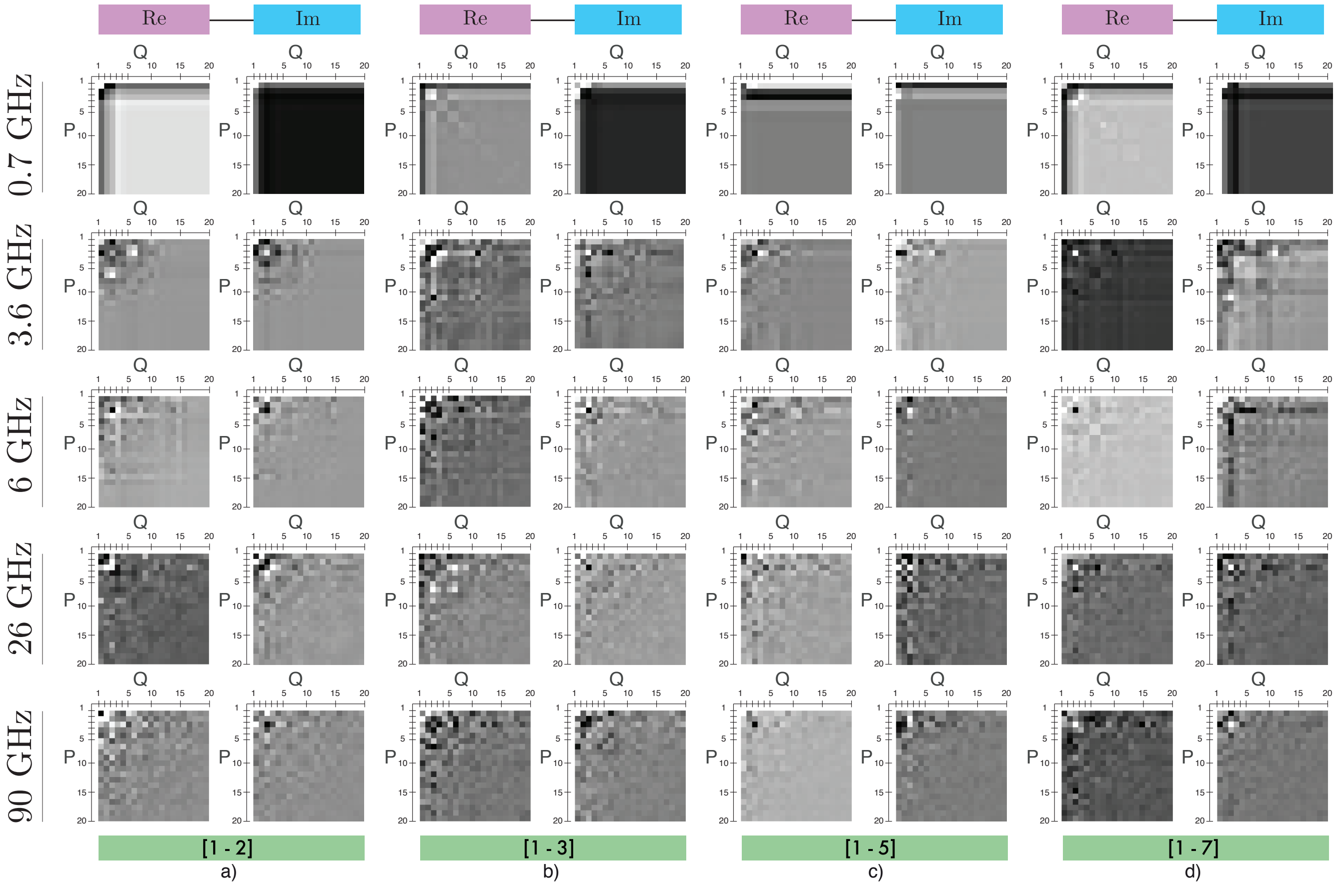

a) b) c) d)

Fig. 6. Effect of increasing frequency. Convergence of real (Re) and imaginary (Im) part of integral A_{mn} depicted on (P, Q)-square. Combination of triangle pairs: a) coplanar far terms $(1-2)$, b) coplanar near terms $(1-3)$, c) orthogonal far terms $(1-5)$, d) orthogonal near terms $(1-7)$.

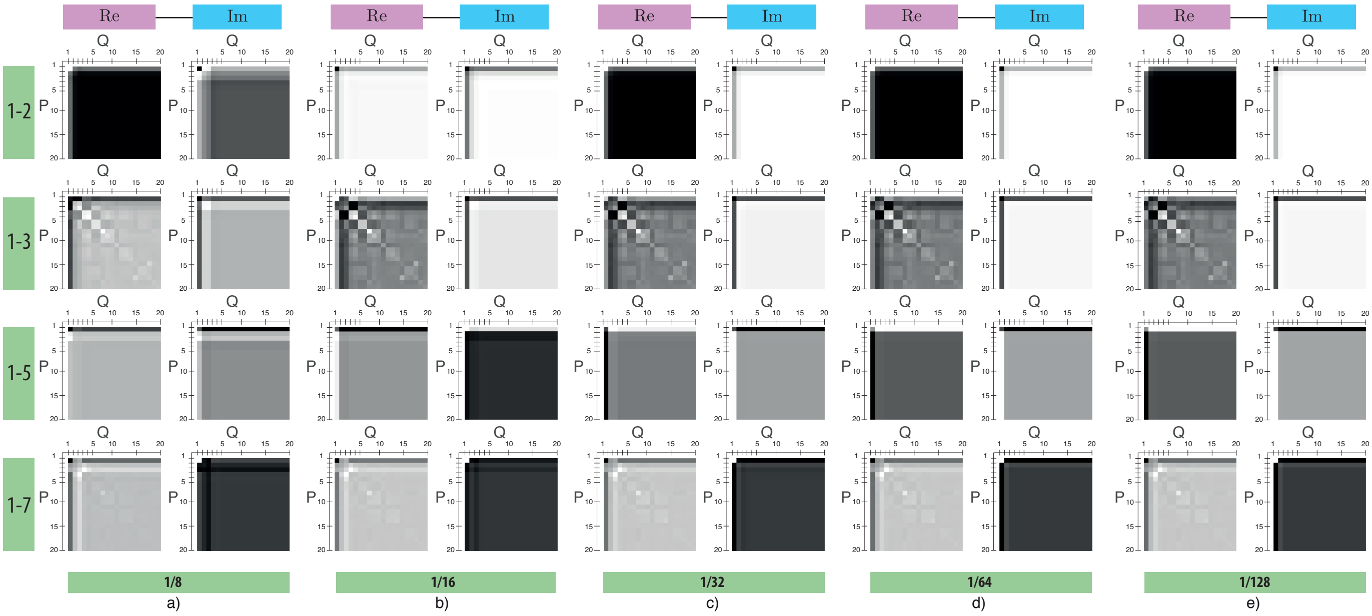

a) b) c) d) e)

Fig. 7. Effect of surface discretization at 3.6 GHz. Convergence of integral A_{mn} with respect to frequency, using several discretization schemes: a) $1/8$, b) $1/16$, c) $1/32$, d) $1/64$, e) $1/128$. Each square (real and imaginary part at particular frequency includes integration orders from $P = 1 \ldots 20, Q = 1 \ldots 20$.

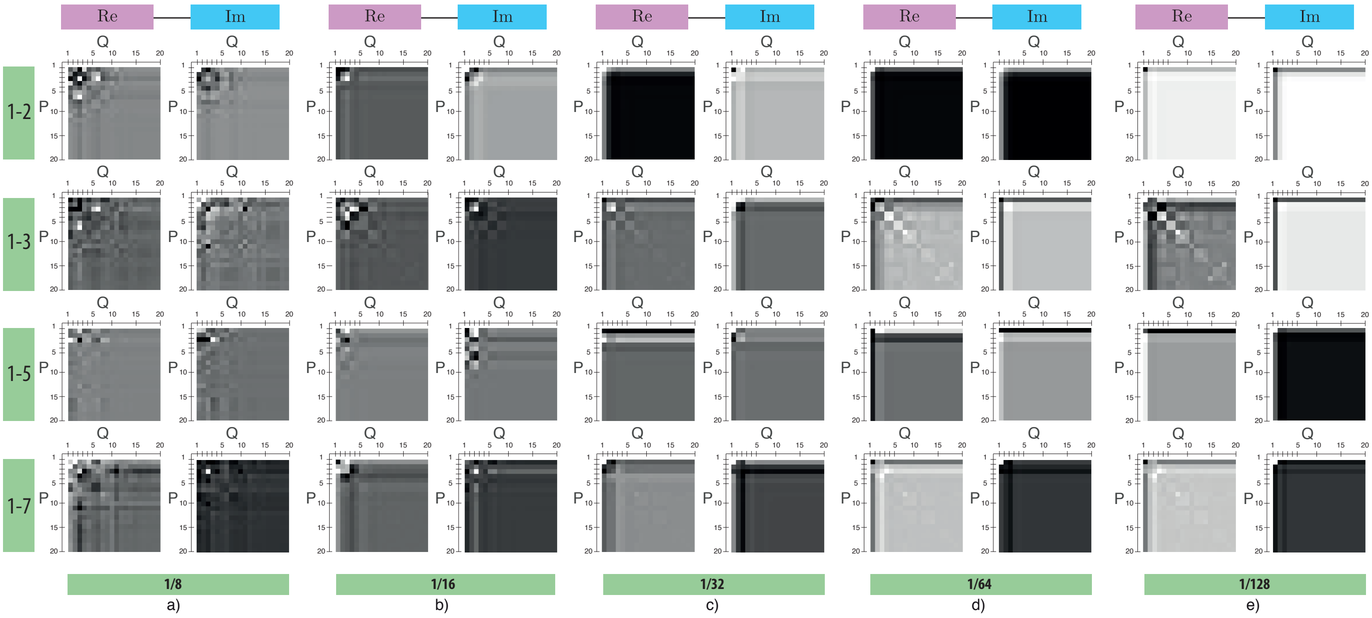

a) b) c) d) e)

Fig. 8. Effect of surface discretization at 26 GHz. Convergence of integral A_{mn} with respect to frequency, using several discretization schemes: a) $1/8$, b) $1/16$, c) $1/32$, d) $1/64$, e) $1/128$. Each square (real and imaginary part at particular frequency includes integration orders from $P = 1 \ldots 20, Q = 1 \ldots 20$.

and 90 GHz) is questionable, at best. On the other hand, using more finer mesh ($1/32$, $1/64$, $1/128$), even at very high frequencies such as 90 GHz, lower integration orders can be used. However, simply utilizing a more finer mesh, results in the significantly increased computational requirements, due to a fully populated system matrices arising from the use of integral equation formulations.

D. Relative Error

Finally, the decision about which level of discretization should be used, will depend not only on the required level of accuracy but also on the computational resources available. This will be illustrated in the following.

The results from the previous sections will be utilized, hence, we consider: five frequencies (0.7 GHz, 3.6 GHz, 6 GHz, 26 GHz, 90 GHz), five discretization schemes ($1/8$, $1/16$, $1/32$, $1/64$, $1/128$), and four triangle interaction types (far and near, coplanar and orthogonal, respectively).

All the results, shown on Figs. 10 and 11, are represented as relative error with respect to reference value according to:

$$\text{Relative error} = \frac{|I_{\text{quadrature}} - I_{\text{reference}}|}{|I_{\text{reference}}|} \tag{12}$$

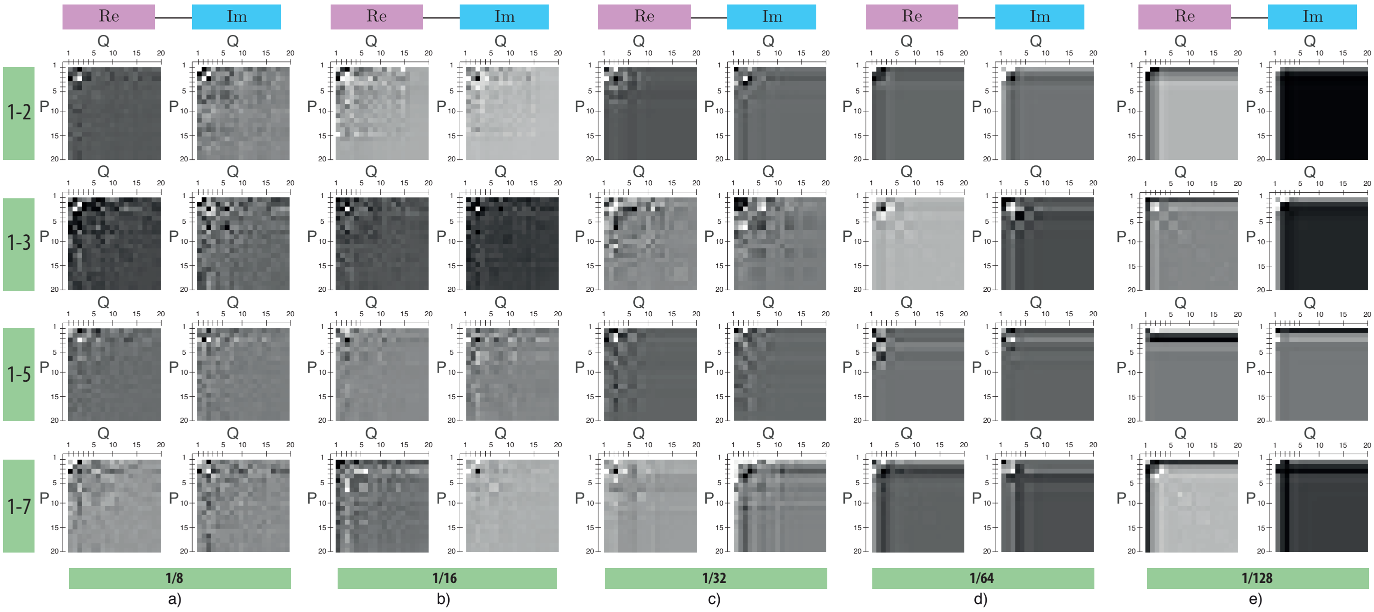

Fig. 9. Effect of surface discretization at 90 GHz. Convergence of integral A_{mn} with respect to frequency, using several discretization schemes: a) $1/8$, b) $1/16$, c) $1/32$, d) $1/64$, e) $1/128$. Each square (real and imaginary part at particular frequency includes integration orders from $P = 1 \ldots 20, Q = 1 \ldots 20$.

where $I_{\text{quadrature}}$ denotes the value at particular quadrature order (P,Q), while $I_{\text{reference}}$ is the reference value selected as the highest integration order, i.e. $P = 20, Q = 20$.

Fig. 10 depicts the convergence vis-à-vis relative error in case of far triangle pairs, $(1-2)$ and $(1-5)$, while on Fig. 11 similar results are shown for near triangle pairs, $(1-3)$ and $(1-7)$.

From Fig. 10, in case of both coplanar and orthogonal far terms, we can see a very rapid convergence with respect to increasing integration order, on both real and imaginary part of the solution. Moreover, it can be seen from Fig. 10 that finer discretization ($1/32$) results in rather similar convergence rate regardless of the frequency. Compared to that, coarser discretization ($1/8$), i.e. larger size of triangular elements, results in rather low convergence rate. This becomes particularly pronounced as the frequency is increased, as the coarser discretization schemes will result in a rather large relative error, i.e. slower solution convergence, even when highest integration order is utilized.

For example, if the required relative error is below $\epsilon = 10^{-5}$, at frequencies below 6 GHz, the choice between using finer discretization versus higher integration rule is still open. However, at 26 GHz and above, the only option is to use finer mesh discretization, as even the highest quadrature rules converge very slowly. Hence, depending on the required accuracy, i.e. relative error, at higher frequencies the only option is to utilize finer discretization resulting in higher number of triangular elements, and consequently, larger system matrix.

On the other hand, in case of near terms, as shown on Fig. 11, although the relative error on the imaginary part falls exponentially, it is nearly constant on the solution's real part, irrespective of the utilized frequency as well as the discretization scheme, suggesting other approach rather than purely numerical one should be considered.

E. Computational Considerations

From the previous analysis, we have seen that in some cases it is not a straightforward decision whether to use finer discretization or to utilize higher integration order. As already mentioned, finer discretization raises the computational requirements, related both to matrix fill time as well as matrix storage.

In Table I parameters of the unit cube are given when unit cube is scaled using several iteration steps n, $n = 1, \ldots, 8$, namely, triangles per unit cube are given, number of the related triangle interactions (pairs) per cube side, as well as the total number of RWG elements (pairs). Finally, Table I shows the resulting matrix size and the memory allocation, for the considered discretization schemes.

Table I shows that as the number of elements is increased, the memory allocation becomes significant burden at finest discretizations ($1/64$, $1/128$), while even relatively coarse discretizations such as $1/16$ and $1/32$ result in matrix size where iterative solution procedures such as GMRES should be considered.

The number of matrix elements and the related matrix size in GB, when double precision is used, are shown on Fig. 12.

As shown on Fig. 12b), simply using finer mesh discretization results in a very high number of matrix elements, and thus prohibitively large requirements for the memory allocation.

Another important thing to consider is the time required to fill the system matrix, which is directly related to the number of elements as well as the number of operations, again related to integration order. Fig. 13 shows the normalized CPU time dependent on the combination of integration orders P and Q.

As seen from Fig. 13, obtained as an average value of 10.000 runs for each (P,Q) combination, selecting lower integration orders, even with modest number of integration points, the computational time can be reduced in half. Again,

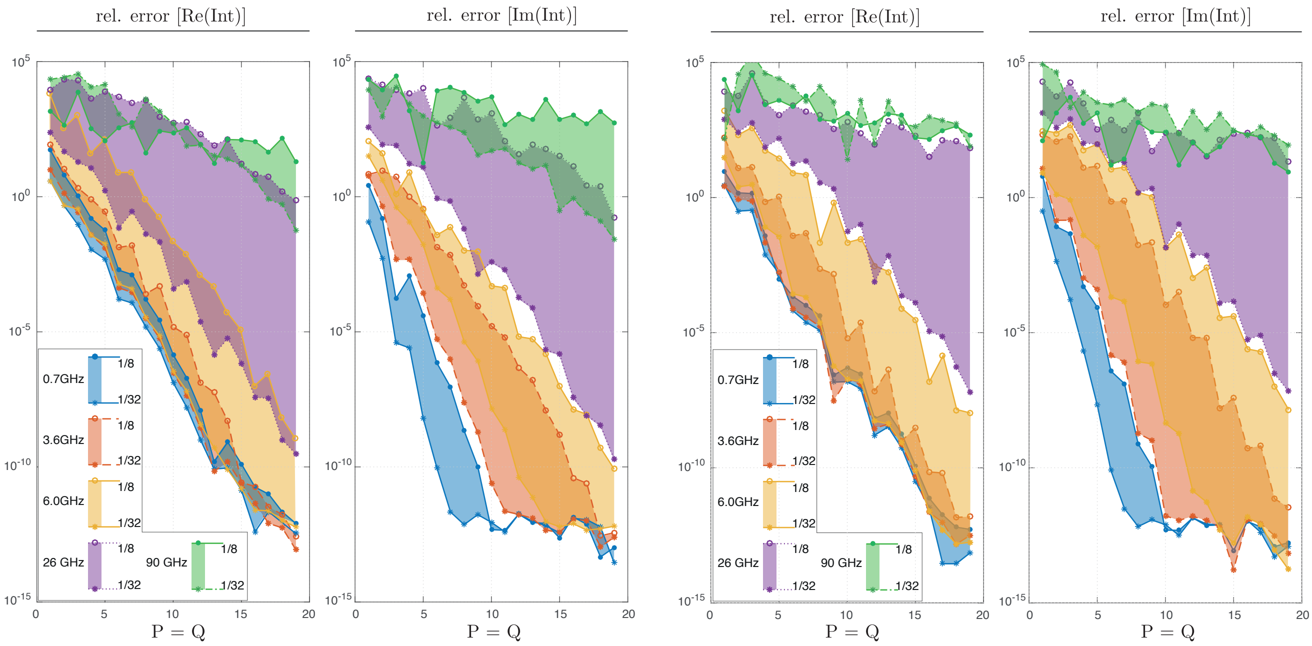

a) b) c) d)

Fig. 10. Far triangle terms convergence: coplanar pair $(1-2)$, a) real part, and b) imaginary part, orthogonal pair $(1-5)$, c) real part, and d) imaginary part. All relative errors obtained with respect to $P=20, Q=20$ integration rule, using discretization schemes $(1/8,\ 1/16,\ 1/32)$ at several 5G frequencies. All x-axes denote $P=Q=1\ldots20$.

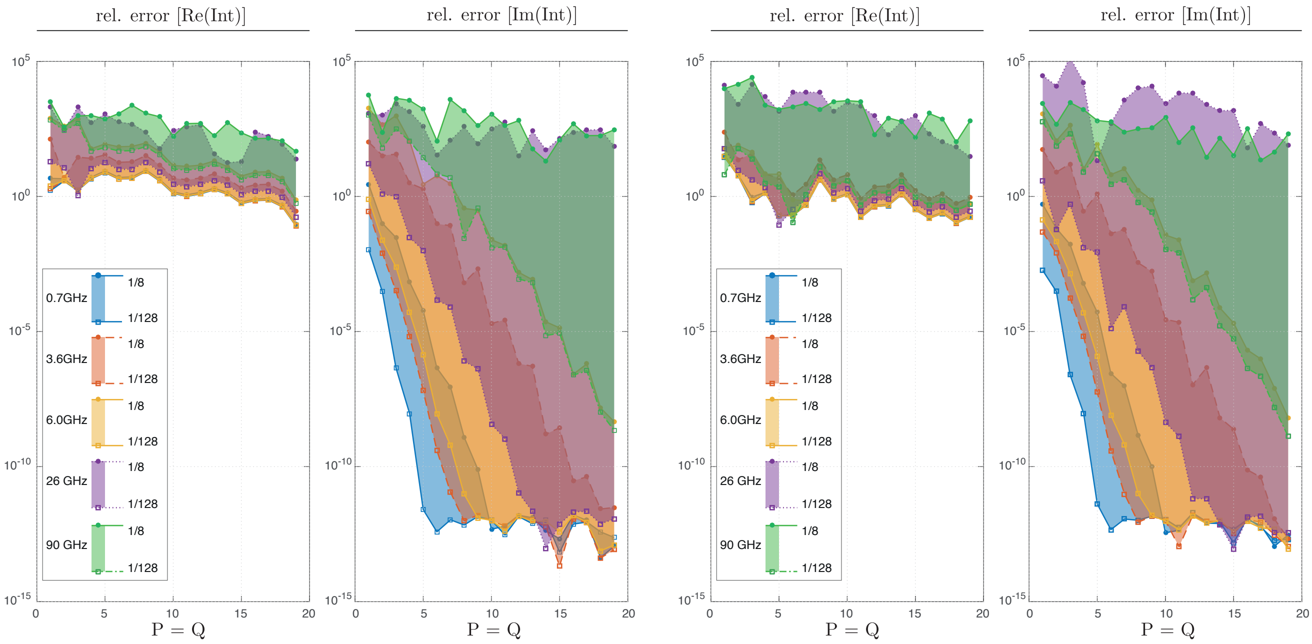

a) b) c) d)

Fig. 11. Near triangle terms convergence: coplanar pair $(1-3)$, a) real part, and b) imaginary part, orthogonal pair $(1-7)$, c) real part, and d) imaginary part. All relative errors obtained with respect to $P=20, Q=20$ integration rule, using discretization schemes $(1/8,\ 1/16,\ 1/32,\ 1/64,\ 1/128)$ at several 5G frequencies. All x-axes denote $P=Q=1\ldots20$.

TABLE I

PARAMETERS OF UNIT CUBE AND RELATED NUMBER OF ELEMENTS: n - SCALING ITERATION; k - SCALING FACTOR; T - TRIANGLES PER UNIT CUBE SIDE; L - NUMBER OF SPECIFIC TRIANGLE INTERACTIONS PER CUBE SIDE; N - TOTAL NUMBER OF RWG ELEMENTS (FOR CUBE); N_Z - NUMBER OF ELEMENTS OF SYSTEM MATRIX; MEMORY ALLOCATION FOR SYSTEM MATRIX.

	k	$T = 2^{2n+1}$	$L = [n\cdot(n-1)+1]^2$	$N = 6T\cdot 3/2$	$N_Z = (2N)^2$	Memory
$n=1$	$1/1$	8	1	72	20.736	165 KB
$n=2$	$1/2$	32	9	288	331.776	2,65 MB
$n=3$	$1/4$	128	49	1152	5.308.416	42,4 MB
$n=4$	$1/8$	512	169	4608	84.934.656	679,5 MB
$n=5$	$1/16$	2048	441	18.432	1.35 E09	10,87 GB
$n=6$	$1/32$	8192	961	73.728	2.17 E10	173,9 GB
$n=7$	$1/64$	32.768	1849	294.912	3.47 E11	2,78 TB
$n=8$	$1/128$	131.072	3249	1.179.648	5.56 E12	44,53 TB

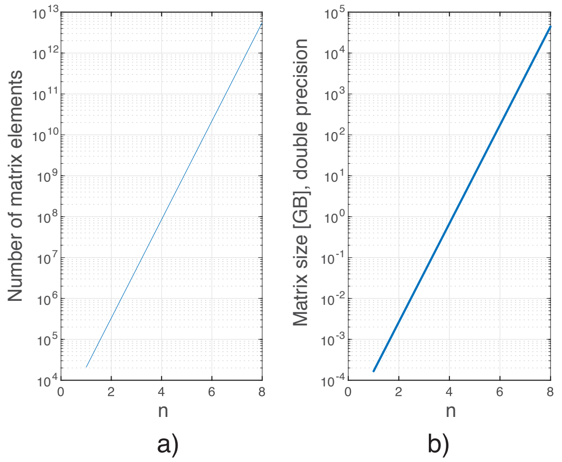

Fig. 12. a) Number of system matrix elements and b) resulting memory allocation in GB using the double precision, depending on the scaling iteration number $n = 1, \ldots, 8$.

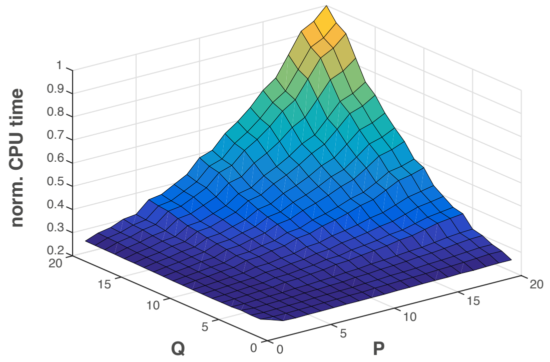

Fig. 13. Normalized CPU time wrt. $P = 20, Q = 20$ integration rule. Value for each P,Q combination obtained as an averaged time of 10.000 runs.

the decision for this will depend on the required calculation precision, as previously discussed.

F. Example of Optimal Integration Order Selection

Finally, the question as to which integration order to select should be addressed. This can be illustrated on the following example, as shown on Fig. 14, where each field from the square denotes the total number of integration points used on both triangles. So, for example, at integration order P=7, 13 integration points are used per triangle, hence, 26 points in total for $(P, Q) = (7, 7)$.

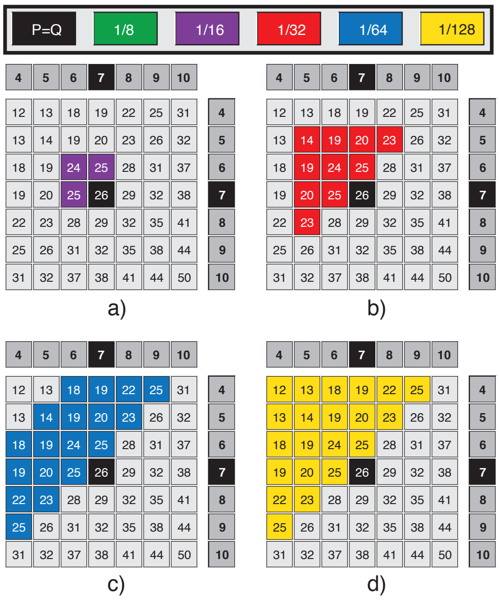

4	5	6	7	8	9	10	
12	13	18	19	22	25	31	4
13	14	19	20	23	26	32	5
18	19	24	25	28	31	37	6
19	20	25	26	29	32	38	7
22	23	28	29	32	35	41	8
25	26	31	32	35	38	44	9
31	32	37	38	41	44	50	10

a)

4	5	6	7	8	9	10	
12	13	18	19	22	25	31	4
13	14	19	20	23	26	32	5
18	19	24	25	28	31	37	6
19	20	25	26	29	32	38	7
22	23	28	29	32	35	41	8
25	26	31	32	35	38	44	9
31	32	37	38	41	44	50	10

b)

4	5	6	7	8	9	10	
12	13	18	19	22	25	31	4
13	14	19	20	23	26	32	5
18	19	24	25	28	31	37	6
19	20	25	26	29	32	38	7
22	23	28	29	32	35	41	8
25	26	31	32	35	38	44	9
31	32	37	38	41	44	50	10

c)

4	5	6	7	8	9	10	
12	13	18	19	22	25	31	4
13	14	19	20	23	26	32	5
18	19	24	25	28	31	37	6
19	20	25	26	29	32	38	7
22	23	28	29	32	35	41	8
25	26	31	32	35	38	44	9
31	32	37	38	41	44	50	10

d)

Fig. 14. Comparison of $(P, Q) = (7, 7)$ with lower integration orders with respect to discretization scheme: a) $1/16$ - purple, b) $1/32$ - red, c) $1/64$ - blue, d) $1/128$ - yellow. All coloured fields denote lower relative error compared to $(P, Q) = (7, 7)$.

For each (P, Q) combination, the relative error with respect to reference value is determined according to (12). All the coloured fields, at the respective discretization scheme, denote the integration order with lower relative error compared to considered $(P, Q) = (7, 7)$ order. The reference value at $(P, Q) = (7, 7)$ is obtained using $1/8$ discretization scheme.

Examples of several integration orders, namely $(P, Q) = (7, 7), (8, 8), (9, 9), (10, 10)$, and $(11, 11)$, are considered at discretization schemes ($1/8$ - green, $1/16$ - purple, $1/32$ - red, $1/64$ - blue, $1/128$ - yellow). All the coloured fields denote the integration order with lower relative error compared to considered $P = Q$ order.

For example, consider situation where $(P, Q) = (7, 7)$ includes 26 integration points calculated at $1/8$ discretization level. At the discretization level $1/32$, as shown on Fig. 14b), all the red coloured fields denote integration orders with lower relative error compared to $(P, Q) = (7, 7)$. Hence, the number of integration points in this case seems to be almost halved, if only the integration points are considered. However, the more accurate results were obtained at $1/32$ discretization scheme, were there are 16 times more triangles compared to $1/8$ scheme, if the uniform mesh such as unit cube is considered. Thus, this would contradict the previous statement about the achieved savings. However, in many cases, it will not be possible to have such as uniform mesh, as triangle element size will be dictated not only by the problem frequency but also by the geometry of the particular problem. In such cases, it will be possible and even necessary to use the more adaptive approach.

Similar results could be obtained for other discretization schemes. These results suggest that, depending on the discretization scheme, it is possible to use lower integration order and thereby, reducing the matrix fill time without actually sacrificing the solution accuracy.

IV. CONCLUSION

In this paper, the suitability of numerical integration of the double surface integral on various combinations of coplanar and orthogonal triangles was investigated using a unit cube test. Several examples of far triangles and near triangles sharing an edge are considered at frequencies related to 5G systems. The results show that the numerical solution at frequencies from the higher GHz range require the use of higher quadrature orders as well as finer discretization schemes, resulting in significantly increased requirements for matrix storage as well as matrix fill time. On the other hand, at lower GHz range, results suggest that when Dunavant's quadrature rules for triangles are utilized, depending on the discretization scheme, lower integration orders could be used, thereby facilitating the decrease of matrix fill time without actually lowering the accuracy of the solution. Further investigation should be carried out to examine how the (P, Q)-square convergence tests could be facilitated to automate the selection of the most suitable numerical integration order, both in terms of accuracy and efficiency.

REFERENCES

[1] IEEE, "IEEE Standard for safety levels with respect to human exposure to electric, magnetic, and electromagnetic fields, 0 Hz to 300 GHz," *IEEE Std C95.1-2019 (Revision of IEEE Std C95.1-2005)*, pp. 1–312, 2019.

[2] ICNIRP, "Guidelines for limiting exposure to electromagnetic fields (100 kHz to 300 GHz)," *Health Physics*, vol. 118, no. 5, pp. 483–524, 2020.

[3] A. Šušnjara, H. Dodig, D. Poljak, and M. Cvetković, "Stochastic-deterministic thermal dosimetry below 6 GHz for 5G mobile communication systems," *IEEE Transactions on Electromagnetic Compatibility*, vol. 63, no. 5, pp. 1667–1679, 2021.

[4] D. Poljak and M. Cvetković, *Human Interaction with Electromagnetic Fields: Computational Models in Dosimetry*. Academic Press, 2019.

[5] D. B. Davidson, *Computational electromagnetics for RF and microwave engineering*. Cambridge University Press, 2010.

[6] Y. Saad and M. H. Schultz, "GMRES: A generalized minimal residual algorithm for solving nonsymmetric linear systems," *SIAM Journal on scientific and statistical computing*, vol. 7, no. 3, pp. 856–869, 1986.

[7] R. Novak, "Viability of numerical full-wave techniques in telecommunication channel modelling," *Journal of Communications Software and Systems*, vol. 16, no. 4, pp. 269–278, 2020.

[8] S. Peng and Z. Nie, "Acceleration of the method of moments calculations by using graphics processing units," *IEEE Transactions on Antennas and Propagation*, vol. 56, no. 7, pp. 2130–2133, 2008.

[9] T. Eibert and V. Hansen, "On the calculation of potential integrals for linear source distributions on triangular domains," *IEEE Transactions on Antennas and Propagation*, vol. 43, no. 12, pp. 1499–1502, 1995.

[10] M. M. Botha, "A family of augmented duffy transformations for near-singularity cancellation quadrature," *IEEE Transactions on Antennas and Propagation*, vol. 61, no. 6, pp. 3123–3134, 2013.

[11] P. Arcioni, M. Bressan, and L. Perregrini, "On the evaluation of the double surface integrals arising in the application of the boundary integral method to 3-D problems," *IEEE Transactions on Microwave Theory and Techniques*, vol. 45, no. 3, pp. 436–439, 1997.

[12] M. Cvetković, D. Poljak, A. L. Kapetanović, and H. Dodig, "Unit cube test for double surface integrals in frequency domain integral equation formulations," in *2021 6th International Conference on Smart and Sustainable Technologies (SpliTech)*. IEEE, 2021, pp. 1–6.

[13] ——, "Study on the suitability of numerical integration at 5G frequencies using unit cube test," in *2021 International Conference on Software, Telecommunications and Computer Networks (SoftCOM)*. IEEE, 2021, pp. 1–6.

[14] S. Rao, D. R. Wilton, and A. Glisson, "Electromagnetic scattering by surfaces of arbitrary shape," *IEEE Transactions on Antennas and Propagation*, vol. 30, no. 3, pp. 409–418, May 1982.

[15] M. Cvetković and D. Poljak, "An efficient integral equation based dosimetry model of the human brain," in *Proceedings of 2014 International Symposium on Electromagnetic Compatibility (EMC EUROPE) 2014, Gothenburg, Sweden, 1-4 September 2014*, 2014, pp. 375–380.

[16] M. Cvetković, D. Poljak, M. Rogić Vidaković, and Z. Dogaš, "Transcranial magnetic stimulation induced fields in different brain models," *Journal of Electromagnetic Waves and Applications*, vol. 30, no. 14, pp. 1820–1835, 2016.

[17] M. Cvetković and D. Poljak, "Electromagnetic-thermal dosimetry comparison of the homogeneous adult and child brain models based on the SIE approach," *Journal of Electromagnetic Waves and Applications*, vol. 29, no. 17, pp. 2365–2379, 2015.

[18] M. Cvetković, S. Lallechere, K. E. Khamlichi Drissi, P. Bonnet, and D. Poljak, "Stochastic sensitivity in homogeneous electromagnetic-thermal dosimetry model of human brain." *Applied Computational Electromagnetics Society Journal*, vol. 31, no. 6, 2016.

[19] M. Cvetković, D. Poljak, and J. Haueisen, "Analysis of transcranial magnetic stimulation based on the surface integral equation formulation," *Biomedical Engineering, IEEE Transactions on*, vol. 62, no. 6, pp. 1535–1545, June 2015.

[20] B. Jung, T. K. Sarkar, and Y.-S. Chung, "A survey of various frequency domain integral equations for the analysis of scattering from three-dimensional dielectric objects," *Progress In Electromagnetics Research-PIER*, vol. 39, no. 193–246, 2002.

[21] B. H. Jung, T. K. Sarkar, S. W. Ting, Y. Zhang, Z. Mei, Z. Ji, M. Yuan, A. De, M. Salazar-Palma, and S. M. Rao, *Time and Frequency Domain Solutions of EM Problems Using Integral Equations and a Hybrid Methodology*. John Wiley & Sons, Inc., Hoboken, New Jersey, 2010.

[22] M. Cvetković, D. Poljak, and K. E. K. Drissi, "Some computational aspects of calculation of integrals arising within the framework of method of moments-application to bioelectromagnetics," in *2016 22nd International Conference on Applied Electromagnetics and Communications (ICECOM)*. IEEE, 2016, pp. 1–6.

[23] D. A. Dunavant, "High degree efficient symmetrical gaussian quadrature rules for the triangle," *International Journal for Numerical Methods in Engineering*, vol. 21, no. 6, pp. 1129–1148, 1985.

[24] P. C. Hammer, O. J. Marlowe, and A. H. Stroud, "Numerical integration over simplexes and cones," *Mathematical Tables and Other Aids to Computation*, vol. 10, no. 55, pp. 130–137, 1956.

[25] P. Silvester, "Symmetric quadrature formulae for simplexes," *Mathematics of Computation*, vol. 24, no. 109, pp. 95–100, 1970.

[26] G. R. Cowper, "Gaussian quadrature formulas for triangles," *International Journal for Numerical Methods in Engineering*, vol. 7, no. 3, pp. 405–408, 1973.

[27] S. Wandzura and H. Xiao, "Symmetric quadrature rules on a triangle," *Computers and Mathematics with Applications*, vol. 45, no. 12, pp. 1829–1840, 2003.

[28] L. Zhang, T. Cui, and H. Liu, "A set of symmetric quadrature rules on triangles and tetrahedra," *Journal of Computational Mathematics*, vol. 27, no. 1, pp. 89–96, 2009.

[29] J. S. Savage and A. F. Peterson, "Quadrature rules for numerical integration over triangles and tetrahedra," *IEEE Antennas and Propagation Magazine*, vol. 38, no. 3, pp. 100–102, 1996.

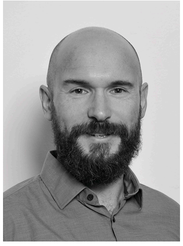

Mario Cvetković was born in 1981. He received the B.S. degree in electrical engineering from the University of Split, Split, Croatia, in 2005, the M.Phil. degree in engineering and electrical engineering from the Wessex Institute of Technology, University of Wales, Cardiff, U.K., in 2009, and the Ph.D. degree in engineering and electrical engineering from the University of Split, in 2013. He is currently an Assistant Professor with the Faculty of Electrical Engineering, Mechanical Engineering, and Naval Architecture (FESB), University of Split, where he teaches the fundamentals of the electrical engineering course. He has authored or coauthored 70 papers in international journals, conference proceedings, and several book chapters. In 2019, he coauthored a book entitled Human Interaction with Electromagnetic Fields - Computational Models in Dosimetry (St. Louis, MO, USA: Elsevier, 2009). His research interests include numerical modeling with finite elements and method of moments, computational bioelectromagnetics, and heat transfer related phenomena. Dr. Cvetkovic is a Member of the International Committee on Electromagnetic Safety (ICES) Technical Committee 95. He was the recipient of the Best Student Paper Award, awarded at the 16th Edition of the International Conference SoftCOM 2008.

Dragan Poljak received the Ph.D. degree in electrical engineering from the University of Split, Split, Croatia, in 1996. He is a Full Professor with the Department of Electronics and Computing, University of Split. He has authored or coauthored more than 160 journals and 250 conference papers, and authored some books, e.g., two by Wiley, Computational Methods in Electro- magnetic Compatibility: Antenna Theory Approach versus Transmission line Models (Wiley, 2018), Advanced Modeling in Computational Electromagnetic Compatibility (Wiley, 2007), and one by Elsevier, Human Interaction with Electromagnetic Fields: Computational Models in Dosimetry (Academic, 2019). He is currently involved with the ITER Physics EUROfusion Collaboration and with the Croatian Center for Excellence in Research for Technical Sciences. His research interests include computational electromagnetics, electromagnetic compatibility, bioelectromagnetics, and plasma physics. Dr. Poljak is a Member of the Editorial Board of Engineering Analysis with Boundary Elements, Mathematical Problems in Engineering, and IET Science, Measurement, and Technology. From 2013 to 2021, he was a Member of the Board of the Croatian Science Foundation. He is active in several working groups of the IEEE/International Committee on Electromagnetic Safety (ICES) Technical Committee 95, and SC6 EMF Dosimetry Modeling. He was the recipient of several prizes for his achievements, such as the National Prize for Science (2004), Croatian Section of the IEEE Annual Award (2016), Technical Achievement Award of the IEEE EMC Society (2019), and George Green Medal from the University of Mississippi (2021).

Ante Lojić Kapetanović was born in Split, Croatia, in 1995. He received the BSc and MSc degrees in electrical engineering at the Faculty of Electrical Engineering, Mechanical Engineering, and Naval Architecture (FESB), University of Split, Croatia, in 2017 and 2019, respectively. From 2020, he has been pursuing a PhD degree in computational bioelectromagnetics at the University of Split. Ante did a three-month research visit at the Aalborg University, Denmark during his MSc, and a one-month research visit at the IETR/CNRS, France. Ante has authored or co-authored 1 journal and over 10 conference papers in different areas of computational sciences. His research interests include computational dosimetry, electromagnetic compatibility of a biological neuron and neural networks, modelling the biological dynamical systems and system identification, and scientific machine learning-emerging methods such as physics-informed neural networks. The focus of the research, however, is human exposure to electromagnetic fields, especially in the mmWave range. Since 2020, Ante has been a member of the Croatian Chapter of the IEEE EMC Society, and from 2021, he has been a student member of the European Bioelectromagnetics association (EBEA).

Hrvoje Dodig (M'18) received a B.Sc. EE degree from the Faculty of Electrical Engineering, Mechanical Engineering and Naval Architecture (FESB) at the University of Split, Croatia in 2002. He was awarded the Chevening scholarship grant for post-graduate study in computational electromagnetics at the Wessex Institute of Technology, UK and received a M.Sc. EE degree from both the Wessex Institute of Technology, UK and the Faculty of Electrical Engineering, Mechanical Engineering and Naval Architecture (FESB) at the University of Split, Croatia in 2005. He received his Ph.D. EE degree from the Wessex Institute of Technology, UK in 2012. From 2013 to 2016 he was with the Department of Radar Technology at the Naval Electronic Center, Croatia, and he was the head of hardware and software design of military communication equipment. Since 2016 he is lecturer at the Department of Naval Electronic and Information Technology at University of Split (PFST). He became assistant professor in 2018 and he teaches electronic circuits, robotics, software design, and algorithms. From 2018-2021 was vice dean of research. His research interests include numerical modelling of electromagnetic fields, boundary and finite element methods, hybrid numerical methods, electromagnetic compatibility, electromagnetic scattering problems and the development of general electromagnetic theory.